

# Getting Air: Modelling and Control of a Hybrid Pneumatic-Electric Legged Robot

Christopher Mailer<sup>1</sup>, Stacey Shield<sup>1</sup>, Reuben Govender<sup>2</sup> and Amir Patel<sup>1</sup>, *Senior Member, IEEE*

**Abstract**—With their combination of power and compliance, pneumatic actuators have great potential for enabling dynamic and agile behaviors in legged robots, but their complex dynamics impose control challenges that have hindered widespread use. In this paper, we describe the development of a tractable model and characterization procedure of an off-the-shelf double acting pneumatic cylinder controlled by on/off solenoid valves for use in trajectory optimization. With this we are able to generate motions which incorporate both the body and actuator dynamics of our robot *Kemba*: a novel quadrupedal robot prototype with a combination of electric and pneumatic actuators. We demonstrate both a 0.5 m jump and land maneuver, and a maximal 1 m jump, approximately 2.2 times its leg length, on the physical hardware with the proposed model and approach. The hardware matches the desired trajectory with a maximum height error of only 5 cm without any feedback on the pneumatic joints, demonstrating the utility of the model in high-level motion generation, and capability of the physical robot.

## I. INTRODUCTION

Powerful, robust actuation is vital for dynamic legged locomotion. Pneumatic actuators have a number of advantages that recommend them for this purpose: in addition to their high force-to-weight ratio and inherent compliance due to the compressibility of air, they are relatively inexpensive and mechanically simple. They can be mounted directly to the joint being actuated, eliminating the need for gearboxes and transmission linkages, as well as the associated inertia and backlash. Repeated collisions between the feet and ground are an essential aspect of legged locomotion, making impact resistance critical for legged robots, particularly when performing agile dynamic maneuvers [1]. Geared transmissions are limited in their maximum reduction ratio [2] or require additional series elastic elements [3] to guarantee impact robustness whilst still producing the high required joint torques.

Pneumatic actuators are also backdrivable due to their direct and low transmission inertia which also improves their force transparency - a crucial component of legged robot control [2]. The chamber pressure also provides a direct measurement of the force produced at the output (once friction has been accounted for) without the need for expensive force transducers.

The hopping robots described in Raibert's seminal publication, *Legged Robots that Balance*, provided a strong early

\*This work was supported by the National Research Foundation (NRF) of South Africa grant number 137762.

Authors are with the <sup>1</sup>Department of Electrical Engineering at the University of Cape Town, and the <sup>2</sup>Department of Mechanical Engineering at the University of Cape Town, South Africa. Corresponding Author: mlrchr001@myuct.ac.za



Fig. 1. *Kemba*, a hybrid electric and pneumatic legged robot designed for rapid maneuvers.

demonstration of the applicability of pneumatic actuation to agile legged robots. Despite this, they were not widely adopted in the field of legged robotics with more mechanically complex hydraulic [4], quasi-direct-drive [1], [5]–[7] and series elastic actuators [3], [8] being used due to their relatively high bandwidth force control capabilities.

The predominant obstacle to their use is that they feature slow dynamics due to the compressibility of air and nonlinear mass flow rates [9] – a formidable challenge for traditional control methods. Different control approaches have been proposed for on/off pneumatic actuators such as sliding mode control [10]–[12] and nonlinear model-predictive control [13], [14]. These are typically used to track reference trajectories for joints [15] and tend to work against the inherent body actuator dynamics rather than allowing them to contribute to efficient locomotion of the robot. A better alternative would be to incorporate the pneumatic actuator dynamics early in the motion planning phase [16]. Trajectory optimization is a promising method of synthesizing viable motion trajectories which incorporate both robot and actuator dynamics. It has a proven track record in the high-level control of agile locomotion in legged robots, with examples of its use including [6], [17]–[20].

In this paper, we present a tractable pneumatic model which enables incorporation of complex pneumatic actuator dynamics at the high level motion planning stage with the

aim of generating feasible motions for *Kemba*: a hybrid electric and pneumatic quadrupedal robot designed with dynamic gait and maneuverability in mind (Fig. 1).

We begin by briefly describing the mechanical design of the robot. We then explain the control scheme, focusing on the development and experimental validation of a tractable pneumatic cylinder model for use in the trajectory optimization problem formulation. Finally, we demonstrate the ability of the robot to track the trajectory effectively through the execution of a vertical jump motion.

## II. HARDWARE PLATFORM

### A. Robot Design

The legged robot *Kemba* aims to combine the best of two actuation schemes, with high torque quasi-direct drive electric motors at the hips for finer fidelity positioning, and high force pneumatic pistons at the knees. This 'half robot' prototype with one foreleg and one hindleg is intended as a platform to investigate explosive transient animal-like motions such as leaping, and accelerating in a bound. Consequently deployment outside of the lab environment has not been considered. The robot weighs approximately 4.3 kg without the support boom, has a body length of 0.5 m, with external power and computing.

The hip actuators are electric motors (TMotor AK70-10) with a single-stage 10:1 planetary gear reduction producing a peak output torque of 24.8 Nm and a maximum speed of 49.7 rad s<sup>-1</sup>. The two knees are actuated by off-the-shelf double-acting pneumatic pistons (Festo DNSU-25-70-PPS-A) with a 25 mm diameter and a 70 mm stroke, attached 48 mm from the knee joint in a 3<sup>rd</sup> class lever arrangement. This lever arm arrangement produces a peak knee torque of approximately 18 Nm. Air to each piston chamber is controlled independently by fast-switching 2-way solenoid valves with a nominal flow rate of 200 L min<sup>-1</sup> providing four discrete operating modes for each piston.

Binary on/off valves are used over proportional valves as they provide an order of magnitude reduction in cost and encourage us to exploit a property of agile manoeuvres where bang-bang control often emerges as the time optimal policy [21], [22]. Air is supplied to the valves at a nominal pressure of  $(0.7 \pm 0.1)$  MPa by a 130 L min<sup>-1</sup> external compressor with a 100 L accumulator tank. Each piston is fitted with a high resolution linear hall effect position sensor (Festo SDAT-MHS) to track the movement of the bore and knee joint. To maximize transient movement capabilities the legs are arranged in an X-Type configuration [23].

### B. Support Boom

The legged robot is connected to the 2.5 m support boom shown in Fig. 2 which serves to restrict the movement of the body to only 3 degrees of freedom, and also provide state information on the position, velocity, and acceleration of the body. The robot can translate vertically and horizontally, and rotate in pitch. Tensioned cables ensure that the robot always remains perpendicular to the ground even as the boom angle changes. State information is provided by three high



Fig. 2. Robot planarizing support boom

resolution encoders on each of the axes and an accelerometer mounted to the end which is fused with a Kalman Filter to provide a full state estimate. Position measurements from the boom are accurate to approximately 0.3 mm. The boom is primarily composed of carbon fiber and weighs 2.7 kg with a rotational inertia about its central pivot of 4.82 kg m<sup>2</sup>, which is significant relative to the mass of the robot. Consequently the dynamics of the boom are also included in the rigid body calculations.

## III. PNEUMATIC ACTUATOR MODEL

In this section, we develop a tractable model of a generic double-acting pneumatic actuator through simplification of an established physics-based model combined with characterization experiments.

### A. Physical Model

A double acting pneumatic actuator is a device with two chambers separated by a sliding bore. We will base our approximate model of this device on the physical model presented in [9] where the pressure dynamics of a single chamber can be described by the following differential equation:

$$\dot{P} = \frac{\kappa RT}{V} \dot{m} + \frac{\kappa \dot{V}}{V} P. \quad (1)$$

The first term describes the change in pressure resulting from a mass flow of air  $\dot{m}$  entering the chamber and the second term describes the change in pressure as a result of the moving bore producing a change in volume  $\dot{V}$ . The flow of air is a function of the valve command  $u \in \{0, 1\}$ , the orifice area  $a$ , and the thin-plate flow function  $\phi()$ :

$$\dot{m} = \begin{cases} u \cdot a \cdot \phi(P_u, P_d) & \text{if } P_u \geq P_d \\ -u \cdot a \cdot \phi(P_d, P_u) & \text{if } P_u < P_d \end{cases} \quad (2a)$$

, where the thin-plate flow function  $\phi()$  is described by:

$$\phi(P_u, P_d) = \begin{cases} \alpha P_u \sqrt{\left(\frac{P_d}{P_u}\right)^{\frac{2}{\kappa}} - \left(\frac{P_d}{P_u}\right)^{\frac{\kappa+1}{\kappa}}} & \frac{P_u}{P_d} \leq \theta \\ \beta P_u & \frac{P_u}{P_d} > \theta \end{cases} \quad (3a)$$

The direction of air flow through the valve and into the chamber switches depending on whether the upstream pressure  $P_u$  or downstream pressure  $P_d$  is greater on either side of the valve orifice, and the flow regime switches depending on whether the pressure difference has exceeded a threshold  $\theta$  and become choked, shown by (3b).  $\alpha$ ,  $\beta$ ,  $\theta$ , and  $\kappa$  are constants.

While this model fully describes the internal dynamics,  $\dot{P}$  and  $\dot{m}$  can both change rapidly and are coupled, making the equations numerically stiff. This requires timesteps on the order of microseconds to integrate which is infeasible for high level motion optimization. To identify and characterize the convergent dynamics of this system, we consider both terms of equation 1 independently and combine their effects to produce the approximated model:

- **Mass flow dynamics:** we simplify this to a first order force/pressure response by considering the pressure response of a single locked volume chamber.
- **Steady-state velocity dynamics:** we consider the combined velocity dependent effects of two opposing chambers and approximate this with a linear damper model. Considering both chambers together is reasonable as the combined chamber volumes are linked with an increase in volume of one chamber having a corresponding decrease in the other.

The justification for these approximations and characterization procedure is detailed in the following sections.

1) *Chamber Force Response:* When a valve state changes, air enters or leaves the piston chamber producing a particular pressure/force response at the output. To characterize this response we connected a force transducer to the output rod which we held stationary, effectively making  $\dot{V} = 0$  and eliminating the second term in (1). By doing so the pressure/force dynamics become a function of the mass flow  $\dot{m}$  through the valve and the chamber volume  $V$ . We expect this response to be dependent on valve state, and the chamber volume. The compressor maintains an output pressure between 0.6 MPa and 0.8 MPa. We performed 5 tests at 0.6 MPa, 0.7 MPa and 0.8 MPa for the two valve states at both the maximum and minimum chamber volumes. This resulted in a total of 60 tests which are summarized in Fig. 3 with the command being sent to the solenoid at  $t = 0s$ .

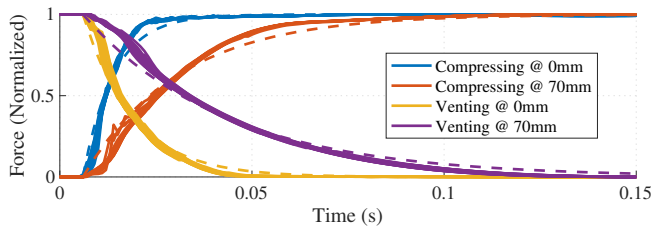


Fig. 3. Normalized force response of a constant volume chamber for compression and venting. Dashed lines show the corresponding first order approximation.

Fig. 3 shows that the response to a venting or compression command is independent of the supply pressure over the tested range, with the 0.6 MPa to 0.8 MPa pressures producing almost identical response curves. The valve switching dead-time is also consistent at 6 ms. The responses can be well approximated by a first-order response as shown by the dashed lines in Fig. 3. The dead-time is included later as described in IV-B. While more complex approximations might provide a marginally better fit, trajectory optimization

will likely be a greater source of inaccuracy with timesteps in the order of 5 ms to 10 ms. We therefore approximate the chamber dynamics with the following first-order differential equation:

$$F = F_{static} \cdot u - \tau \dot{F}, \quad (4)$$

where  $F_{static}$  is the maximum steady-state force produced by the chamber, which is controlled by the valve command  $u \in \{0, 1\}$ , and  $\tau$  is the time constant of the first-order approximation. The time constants of the fitted functions are summarized in Table I.

TABLE I  
CHAMBER FORCE RISE TIME

Chamber Mode	Rise Time	
	$x = 0 \text{ mm}$	$x = 70 \text{ mm}$
Compression ( $u = 1$ )	8 ms	25 ms
Venting ( $u = 0$ )	13 ms	37 ms

The time constant is a function of both the valve mode, and the amount of volume needing to be filled or vented in the chamber. Furthermore, it can be shown that this response time is linearly related to the chamber volume. Fig. 4 shows the pressure response for 5 chamber volume fractions from equation 1 to justify this linear relation.

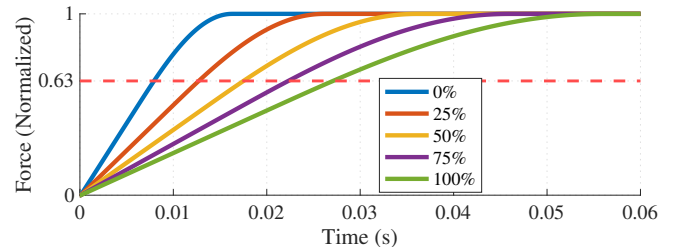


Fig. 4. Chamber force response for the minimum to maximum chamber volumes expressed as a percentage of the volume range

While the rise time is linearly dependent on chamber volume, the valve commands  $u$  are discrete. To ensure the model remains continuous for gradient based methods we also linearly interpolate the rise time for the chamber modes with the discrete states being imposed during trajectory optimization. The rise time can therefore be expressed as the following linear function:

$$\tau(u, x) = \tau_0 + u\tau_1 + x\tau_2 + ux\tau_3 \quad (5)$$

Where  $x$  is the extension of the actuator and the four time constants  $\tau_0, \tau_1, \tau_2, \tau_3$ , are fit directly from the measured data using a bilinear interpolation.

2) *Steady-state Velocity Characterization:* When the piston bore moves, its movement produces a proportional change in the volume of the extend and retract chambers. This change in volume produces a pressure/force change governed by term 2 in (1). To characterize this behavior two identical pistons were arranged opposing each-other with a

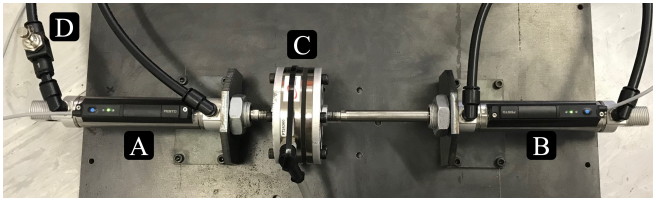


Fig. 5. Piston characterization setup showing the resistance piston (A), the piston being characterized (B), force transducer (Axia80-M20) (C) and flow restricting valve (D)

force transducer in between as shown in Fig. 5. The steady-state force produced by the piston was measured at different velocities by varying the resistance applied by the opposing piston using a flow restricting valve, analogous to a motor dynamometer. Multiple tests were required to fully explore the velocity range achievable by the piston. Fig. 6 shows the force produced by the piston over this velocity range for each of the 4 discrete actuation modes.

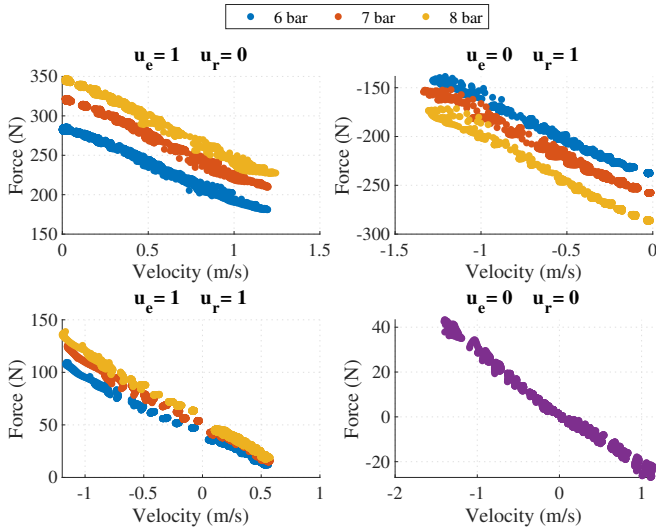


Fig. 6. Force velocity relationship for a double acting pneumatic actuator

Based on these data the actuator behaves almost as a linear damper where the damping constant is a function of the actuation mode. While also a function of supply pressure, we only use the fit for a nominal supply pressure of 0.7 MPa. A linear function was fit to the data in Fig. 6 and the parameters from this are summarized in Table II.

The  $F_{static}$  force corresponds to the steady-state force in (4). The output force of the double acting piston can now be described by the difference in the force produced between the extend and retract chambers with a simple damping term. To ensure that the damping term varies based on the actuation mode, but still remains continuous, we again use a bilinear interpolation. We do not consider this an accurate approximation, but rather chose the simplest interpolation method to maintain continuity and provide a means to transition between states during the optimization procedure.

TABLE II  
PNEUMATIC STEADY-STATE LINEAR FIT

Mode	Supply (MPa)	$F_{static}$ (N)	$c_d$ (Ns/m)	$R^2$
Extend	0.6	287	91	0.992
	0.7	324	97	0.994
	0.8	349	103	0.995
Retract	0.6	-239	78	0.995
	0.7	-260	84	0.989
	0.8	-291	89	0.994
Both	0.6	41	52	0.993
	0.7	50	59	0.989
	0.8	55	64	0.991
Unactuated	0.0	0	25	0.980

$$c_d(u_e, u_r) = c_0 + u_e c_1 + u_r c_2 + u_e u_r c_3 \quad (6)$$

Each of the constants  $c_0$ ,  $c_1$ ,  $c_2$ ,  $c_3$  is found by fitting the bilinear surface to the data in table II. We combine the transient behaviour of the two opposing chambers and the combined damped output behaviour into the following actuator force model:

$$F = F_e(u_e, x_e) - F_r(u_r, x_r) - c_d(u_e, u_r)\dot{x}, \quad (7)$$

where  $F_e()$  and  $F_r()$  are the extend and retract chamber first-order dynamics and  $c_d()$  is the combined damping effect.

We experimented with incorporating the damping effect into the first-order chamber dynamics with a term that modified the static force  $F_{static}$  in (4). However, while a marginally better approximation, we were unable to converge on a feasible solution in optimization. Simplifying the model to a single damping term still served as a sufficient approximation with dramatically better convergence during the trajectory optimization step. To verify the performance of the approximated actuator model we compared it to the force predicted by the physics-based model. To adequately explore the operating region we supplied 10 Hz random Bernoulli distributed valve commands with uniformly distributed random piston position and velocity states. Fig. 7 shows the force predicted by the physics-based model overlaid with the force predicted by the approximated model. Based on this we can expect the motions generated with trajectory optimization to be a close approximation to what is achievable with the real hardware.

#### IV. CONTROL

The pneumatic actuator model for a nominal pressure of 0.7 MPa was incorporated into a trajectory optimization problem that was used to generate a torque-minimizing trajectory for a 0.5 m jump and a 1 m jump. We then executed these trajectories on the robot with a simple feedback controller on the hip and shoulder joints.

##### A. Trajectory Optimization

1) *Problem Formulation:* The problem was formulated using the first-order contact-implicit direct collocation formulation described in [24]. The trajectory consisted of  $N =$

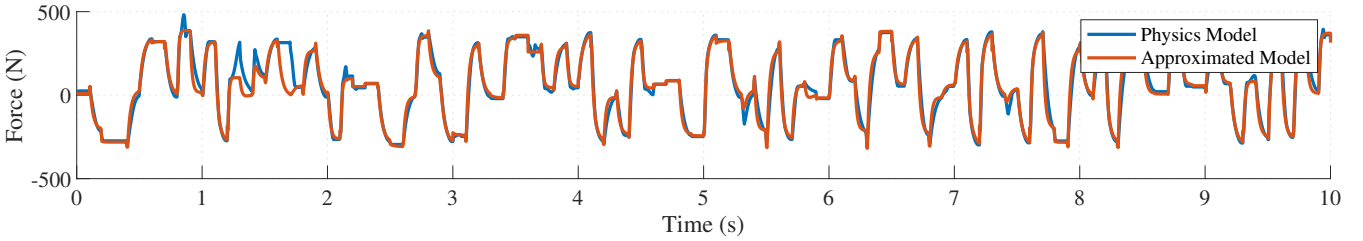


Fig. 7. Predicted actuator force from the proposed model and full dynamics model for random inputs

100 timesteps having a variable duration of  $5 \text{ ms} \pm 20\%$ . This formulation uses complementarity constraints to model unilateral collision behavior – namely, the foot-ground contacts and the hard end stops of the pistons. These constraints were made more tractable using a penalty minimization method [25].

**2) Dynamic Model:** We used the planar rigid-body model illustrated in Fig. 8 to represent the robot. The piston body

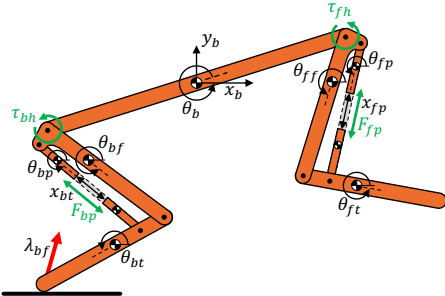


Fig. 8. Robot rigid body arrangement with the absolute angle formulation of the generalized coordinates.

and rod were included as rigid bodies, as they make up a significant fraction of the mass of the leg. The leg with the piston is modeled as a closed kinematic chain, with explicitly-defined constraint forces maintaining the connection between the piston rod and tibia [26]. To simplify the dynamic equations, the angles of each link are referenced to the world frame [26]. The inertial effects of the geared hip rotors and the boom were also included in the dynamic model.

Additional constraints are required to fully integrate the simplified pneumatic actuator model into the trajectory optimization problem. The chamber force dynamics in (4) are explicitly modeled using differential equations, which are solved numerically using the same implicit Euler integration scheme applied to the robot’s equations of motion.

To approximate the switching behavior of the binary solenoid valves, we apply the constraint

$$u_i(1 - u_i) = 0, \quad (8)$$

where  $u_i \in [0, 1]$  is the command being sent to the solenoid valves at the  $i^{\text{th}}$  node. This ensures that the valve can only take on the value 1 or 0 at each timestep which correspond to the *on* or *off* states respectively. As with the other complementarity constraints, we use a penalty minimization method to make this constraint more tractable for the solver.

**3) Jumping Task:** To produce a jump and land motion we specified that the body must start and end horizontal with both feet on the ground, maintain the same  $x$  position, and reach a desired body height at the middle node of the trajectory. The hip motor positions were left unconstrained and the knee pistons were set to start in their fully retracted state. Only the initial and final states of the model were specified, leaving the timing of the valves, movement of the joints, and contact scheduling to the optimizer.

**4) Cost Function:** We applied the following cost function to minimize the torque exerted by the electric motors to perform the jump:

$$J = \sum_{i=1}^N \tau_i^T \tau_i + \rho P_i \quad (9)$$

Where  $\tau_i$  and  $P_i$  are the hip torques and complementarity penalty terms at the  $i^{\text{th}}$  node. As in the MIT Cheetah desk jump [18], the purpose of this optimization was primarily to regularize the torque profiles against chattering. The weight  $\rho$  is set to  $1 \times 10^4$  to prioritize penalty minimization.

**5) Solver:** The optimization problem was written in the Python library Pyomo [27] and had 8982 variables. It was solved using the NLP solver IPOPT [28] with the linear MA86 solver [29] in approximately 55 s on a 2-core laptop.

### B. Trajectory Tracking

From the optimization we get the desired hip motor angles  $q_d$ , velocities  $\dot{q}_d$ , hip torques  $\tau_d$  and valve commands  $u$ . These trajectories are at approximately 200 Hz with some variation due to the variable timestep, however the robot controller executes at a fixed frequency of 1 kHz on an external Speedgoat real-time target machine. We therefore interpolate the trajectories from optimization to match the controller frequency. Each hip motor uses the following controller to track the desired trajectory:

$$\tau = K_p(q_d - q) + K_d(\dot{q}_d - \dot{q}) + \tau_{ff}, \quad (10)$$

where the joint torque commands are used as feed-forward torques  $\tau_{ff}$  with a proportional-derivative (PD) controller to additionally track joint position and velocity. The knee pistons are sent the valve commands shifted forwards by 6 ms to account for the valve dead-time evident in Fig. 3.

Fig. 9 shows the valve commands and motor torques produced by trajectory optimization for the jump and land motion. The pneumatic actuator dynamics can clearly be seen in the expected piston force with force dropping as the knee

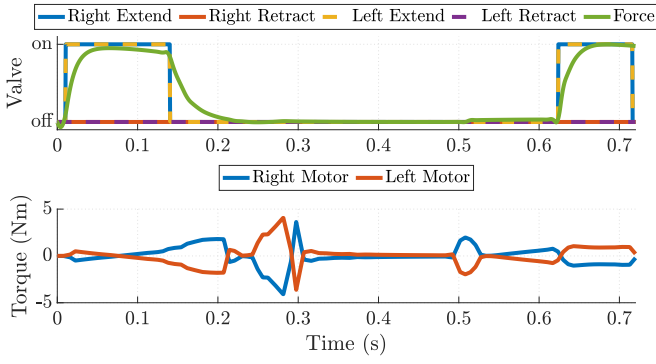


Fig. 9. Valve commands and motor torques resulting from optimization for the 0.5 m jump trajectory.

extends faster. It is worth noting that the solution accounts for the residual actuator force as the chamber vents, by turning off the extend valve even before the feet leave the ground at 0.2 s.

#### V. HARDWARE VALIDATION

We executed the 0.5 m jump and land trajectory shown in Fig. 9 *Kemba*. The body and actuator tracking performance is shown in Fig. 10 and a video of the jumps is included in the supplementary material.

The final jump height is the combined effect of the piston dynamics in the closed kinematic chain arrangement, contact timing, and body dynamics. The similarity between the optimized trajectory and the resulting trajectory on the hardware with a maximum height error of only 3 cm (see Fig. 10) provides a validation of the proposed model and demonstrates its applicability to real hardware.

We additionally attempted a 1 m maximal jump without a landing phase. This height corresponds to roughly twice the leg length of the robot – a considerable height for a robot effectively weighing 7 kg, which illustrates the benefit of the pneumatic actuators towards explosive agility. A video of this jump is also included in the supplementary material and a sequence of frames from the video is shown in Fig. 11.

While our approach results in close to real performance with only open-loop trajectory tracking, model errors are inevitable and will compound throughout the motion. This is evident in Fig. 10 with knee piston tracking deteriorating towards the end of the motion during the landing phase.

#### VI. CONCLUSIONS AND FUTURE WORK

This paper presents a tractable pneumatic cylinder model and trajectory optimization formulation that enables the incorporation of full pneumatic actuator dynamics into high level motion generation. Execution of a generated 0.5 m jump and land trajectory on a prototype electric-pneumatic robot is a further contribution, and demonstrates the validity and utility of the model, and capability of the hardware.

In the hardware experiment, the robot was able to repeatedly execute a 0.5 m vertical jump and land, as well as a maximal 1 m jump by tracking the result of the trajectory optimization. This presents a first step in integrating powerful

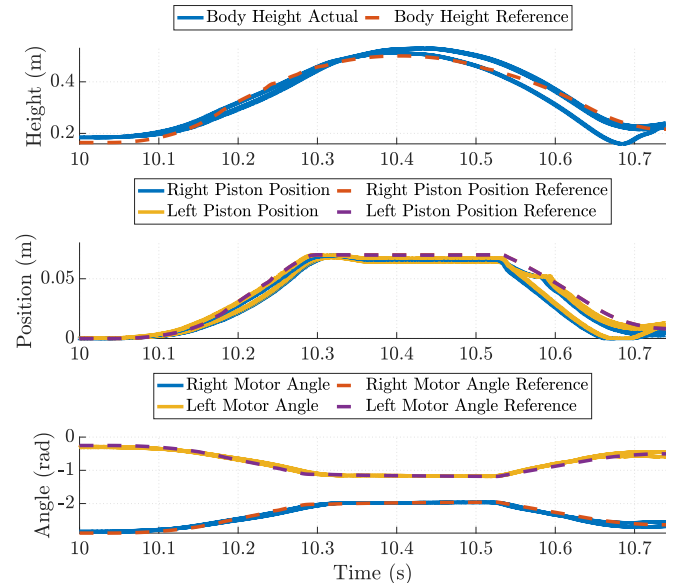


Fig. 10. Body and actuator states on the hardware compared to the reference trajectory for three 0.5 m jumps.

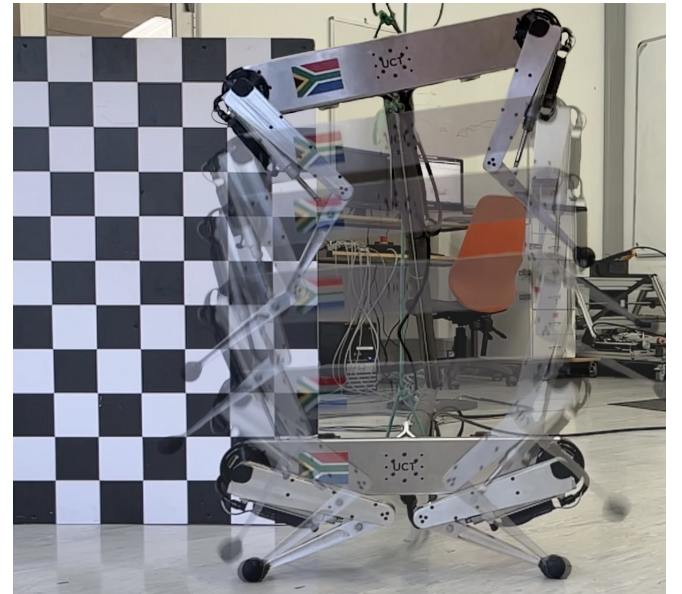


Fig. 11. A sequence of overlaid frames showing the 1 m jump without landing. The squares on the checkerboard are 9 cm and the green rope serves to catch the robot.

and robust pneumatic actuators with modern legged robot control approaches. In future work, we aim to close the loop with a low-level pressure tracking controller for the pneumatics which can perform minor corrections around the nominal trajectory to further improve tracking performance to the level required for executing dynamic motions such as bounding, and jumping over obstacles.

#### ACKNOWLEDGMENT

Author C. Mailer sincerely thanks the Harry Crossley Foundation for their fellowship funding and support of this research.

## REFERENCES

- [1] B. Katz, J. Di Carlo, and S. Kim, “Mini Cheetah: A Platform for Pushing the Limits of Dynamic Quadruped Control,” in *International Conference on Robotics and Automation (ICRA)*. IEEE, 2019, pp. 6295–6301.
- [2] P. M. Wensing, A. Wang, S. Seok, D. Otten, J. Lang, and S. Kim, “Proprioceptive actuator design in the MIT cheetah: Impact mitigation and high-bandwidth physical interaction for dynamic legged robots,” *IEEE Transactions on Robotics*, vol. 33, no. 3, pp. 509–522, 6 2017.
- [3] M. Hutter, C. Gehring, D. Jud, A. Lauber, C. D. Bellicoso, V. Tsounis, J. Hwangbo, K. Bodie, P. Fankhauser, M. Bloesch, R. Diethelm, S. Bachmann, A. Melzer, and M. Hoepflinger, “ANYmal - A highly mobile and dynamic quadrupedal robot,” in *IEEE International Conference on Intelligent Robots and Systems*, vol. 2016-November, 2016, pp. 38–44.
- [4] C. Semini, N. G. Tsagarakis, E. Guglielmino, M. Focchi, F. Cannella, and D. G. Caldwell, “Design of HyQ - A hydraulically and electrically actuated quadruped robot,” *Proceedings of the Institution of Mechanical Engineers. Part I: Journal of Systems and Control Engineering*, vol. 225, no. 6, pp. 831–849, 2011.
- [5] G. Bledd, M. J. Powell, Katz Benjamin, J. Di Carlo, P. M. Wensing, and S. Kim, “MIT Cheetah 3: Design and Control of a Robust, Dynamic Quadruped Robot,” in *IEEE/RSJ International Conference on Intelligent Robots and Systems (IROS)*, 2018, pp. 2245–2252.
- [6] M. Chignoli, D. Kim, E. Stanger-Jones, and S. Kim, “The MIT Humanoid Robot: Design, Motion Planning, and Control for Acrobatic Behaviors,” in *IEEE-RAS International Conference on Humanoid Robots*, vol. 2021-July. IEEE Computer Society, 2021, pp. 1–8.
- [7] J. Yu, J. Hooks, X. Zhang, M. S. Ahn, and D. Hong, “A Proprioceptive, Force-Controlled, Non-Anthropomorphic Biped for Dynamic Locomotion,” in *IEEE-RAS 18th International Conference on Humanoid Robots (Humanoids)*, 2018, pp. 1–9.
- [8] M. Hutter, C. D. Remy, M. A. Hoepflinger, and R. Siegwart, “Scar-IETH: Design and control of a planar running robot,” in *IEEE/RSJ International Conference on Intelligent Robots and Systems*. Institute of Electrical and Electronics Engineers (IEEE), 12 2011, pp. 562–567.
- [9] Y. Tassa, T. Wu, J. Movellan, and E. Todorov, “Modeling and identification of pneumatic actuators,” in *IEEE International Conference on Mechatronics and Automation*. IEEE, 2013, pp. 437–443.
- [10] H.-H. Liou and M.-T. Ho, “Hopping control of a pneumatic single-legged robot using sliding mode control,” in *2019 International Automatic Control Conference (CACS)*. IEEE, 2019, pp. 1–6.
- [11] A. Paul, J. Mishra, and M. Radke, “Reduced Order Sliding Mode Control for Pneumatic Actuator,” *IEEE Transactions on Control Systems Technology*, vol. 2, no. 3, pp. 271–276, 1994.
- [12] T. Nguyen, J. Leavitt, F. Jabbari, and J. E. Bobrow, “Accurate Sliding-Mode Control of Pneumatic Systems Using Low-Cost Solenoid Valves,” *IEEE/ASME Transactions on Mechatronics*, vol. 12, no. 2, pp. 216–219, 2007.
- [13] X. Shen, J. Zhang, E. J. Barth, and M. Goldfarb, “Nonlinear model-based control of pulse width modulated pneumatic servo systems,” *Journal of Dynamic Systems, Measurement and Control, Transactions of the ASME*, vol. 128, no. 3, pp. 663–669, 9 2006.
- [14] H. Qi, G. M. Bone, and Y. Zhang, “Position Control of Pneumatic Actuators Using Three-Mode Discrete-Valued Model Predictive Control,” *Actuators*, vol. 8, no. 3, p. 56, 7 2019.
- [15] E. Todorov, C. Hu, A. Simpkins, and J. Movellan, “Identification and control of a pneumatic robot,” in *IEEE RAS and EMBS International Conference on Biomedical Robotics and Biomechatronics, BioRob*, 2010, pp. 373–380.
- [16] D. J. Braun, F. Petit, F. Huber, S. Haddadin, P. Van Der Smagt, A. Albu-Schäffer, and S. Vijayakumar, “Robots driven by compliant actuators: Optimal control under actuation constraints,” *IEEE Transactions on Robotics*, vol. 29, no. 5, pp. 1085–1101, 2013.
- [17] S. Kuindersma, R. Deits, M. Fallon, A. Valenzuela, H. Dai, F. Permenter, T. Koolen, P. Marion, and R. Tedrake, “Optimization-based locomotion planning, estimation, and control design for the atlas humanoid robot,” *Autonomous Robots*, vol. 40, no. 3, pp. 429–455, 3 2016.
- [18] Q. Nguyen, M. J. Powell, B. Katz, J. D. Carlo, and S. Kim, “Optimized Jumping on the MIT Cheetah 3 Robot,” in *International Conference on Robotics and Automation (ICRA)*, 2019, pp. 7448–7454.
- [19] G. Muscato and G. Spampinato, “A multi level control architecture for a pneumatic robotic leg,” in *2005 IEEE Conference on Emerging Technologies and Factory Automation*, vol. 2, 2005, pp. 7–79.
- [20] M. Bjelonic, C. D. Bellicoso, Y. de Viragh, D. Sako, F. D. Tresoldi, F. Jenelten, and M. Hutter, “Keep rollin’—whole-body motion control and planning for wheeled quadrupedal robots.” *IEEE Robotics and Automation Letters*, vol. 4, no. 2, pp. 2116–2123, 2019.
- [21] C. Hubicki, M. Jones, M. Daley, and J. Hurst, “Do limit cycles matter in the long run? Stable orbits and sliding-mass dynamics emerge in task-optimal locomotion,” in *IEEE International Conference on Robotics and Automation (ICRA)*, vol. 2015-June, no. June, 2015, pp. 5113–5120.
- [22] T. Seyde, I. Gilitschenski, W. Schwarting, B. Stellato, M. Riedmiller, M. Wulfmeier, and D. Rus, “Is Bang-Bang Control All You Need? Solving Continuous Control with Bernoulli Policies,” *Advances in Neural Information Processing Systems*, vol. 34, pp. 27209–27221, 2021.
- [23] L. Raw, C. Fisher, and A. Patel, “Effects of Limb Morphology on Transient Locomotion in Quadruped Robots,” in *IEEE/RSJ International Conference on Intelligent Robots and Systems (IROS)*, 2019, pp. 3349–3356.
- [24] M. Posa, C. Cantu, and R. Tedrake, “A direct method for trajectory optimization of rigid bodies through contact,” *International Journal of Robotics Research*, vol. 33, no. 1, pp. 69–81, 2014.
- [25] Z. Manchester and S. Kuindersma, “Variational Contact-Implicit Trajectory Optimization,” in *Robotics Research*. Springer, 2020, pp. 985–1000.
- [26] A. Knemeyer, S. Shield, and A. Patel, “Minor Change, Major Gains: The Effect of Orientation Formulation on Solving Time for Multi-body Trajectory Optimization,” *IEEE Robotics and Automation Letters*, vol. 5, no. 4, pp. 5331–5338, 2020.
- [27] W. E. Hart, C. D. Laird, J.-P. Watson, D. L. Woodruff, G. A. Hackebeil, B. L. Nicholson, and J. D. Siirola, *Pyomo-optimization modeling in python*. Springer, 2017, vol. 67.
- [28] A. Wächter and L. T. Biegler, “On the implementation of an interior-point filter line-search algorithm for large-scale nonlinear programming,” *Mathematical Programming*, vol. 106, no. 1, pp. 25–57, 5 2006.
- [29] A. HSL, “A collection of Fortran codes for large-scale scientific computation,” See <http://www.hsl.rl.ac.uk>, 2007.